ISSN 1392–1320 MATERIALS SCIENCE (MEDŽIAGOTYRA). Vol. 21, No. 3. 2015

Development of Young's Modulus of Illitic Clay during Heating up to 1100 °C

Tomáš HÚLAN [1,*], Anton TRNÍK [1,2], Igor ŠTUBŇA [1], Peter BAČÍK [3], Tiit KALJUVEE [4], Libor VOZÁR [1]

[1] *Department of Physics, Constantine the Philosopher University, 94974 Nitra, Slovakia*
[2] *Department of Materials Engineering and Chemistry, Czech Technical University, 16629 Prague, Czech Republic*
[3] *Department of Mineralogy and Petrology, Comenius University, 84215 Bratislava, Slovakia*
[4] *Laboratory of Inorganic Materials, Tallinn Technical University, 190 86 Tallinn, Estonia*

crossref http://dx.doi.org/10.5755/j01.ms.21.3.7152

Received 20 May 2015; accepted 24 July 2014

Young's modulus of green illite from Füzérradvány (Hungary) was measured in-situ in the temperature interval 20 °C – 1100 °C and auxiliary analyses DTA, TG and TDA, XRD and EGA, were also performed. It was found that a removal of the physically bound water (20 °C – 250 °C) sets illite crystals closer, which leads to a significant increase of Young's modulus from its initial value of 7 GPa to the maximum 12 GPa at 300 °C. Young's modulus slightly decreases in the temperature interval of dehydroxylation of illite (300 °C – 800 °C), and which then reaches up to 45 GPa at 1100 °C, increasing exponentially as a consequence of the sintering above 800 °C.
Keywords: illite; Young's modulus; physically bound water; dehydroxylation; sintering.

1. INTRODUCTION

Illite is a significant rock forming mineral that is a main component of illitic clay and soil. Its structure consists of the repetition of tetrahedron – octahedron – tetrahedron (T-O-T) sheets in one layer. The interlayer space is occupied mainly by potassium cations, which are responsible for the absence of swelling. Additionally the variable amounts of water molecules lie between the T-O-T layers [1 – 4].

Illitic clays, also called ball clays, are very often used in the manufacturing of traditional ceramics [5 – 9] and geopolymers [10]. Illite is usually mixed not only with other clays but also with microscopic crystals of carbonates, feldspars, micas and quartz and is very rarely found separately in nature.

Almost pure illite was found in the Füzérradvány location in North-Eastern Hungary [11, 12]. This illite was previously studied in [3 – 5, 11, 13, 14] and in other works. It was specified that this illite is of 1M polytype [3, 4]. According to [11] the illite contains 48.51 mass % of SiO_2, 31.26 mass % of Al_2O_3, 7.85 mass % of K_2O and ~ 4.3 mass % of Fe, Ti, Ca, Mg, Na and S oxides. Loss on ignition is ~ 6.9 mass %. The SEM images show individual grains with highly altered or damaged rim structures. In general, mostly hexagonal grains are separated by fractures with variable widths between 1 and 10 μm. The presence of a minor amount of quartz was seen in the CL images and was also confirmed by XRD [15].

Generally, during heating up to 1200 °C, illite goes through several changes. The first of which is a loss of physically bound water which takes place between room temperature and 300 °C [16, 17]. Because H_2O is bound to T-O-T clay minerals in different ways, the loss of the physically bound water occurs in overlapping temperature intervals. For illite, two DTA endothermic minima were observed in this temperature region [16].

The next process is dihydroxylation, which begins at ~ 450 °C [2, 13, 16 – 18] and is accompanied with mass loss of 5.2 – 5.6 mass % [17] and no shrinking [17 – 19]. It is still not possible to reach a unique definition because there are several possible models of the mechanism reaction of the illite dehydroxylation [13]. An Arrhenius plot showed two slopes which gave two values of the activation energy 697 kJ mol^{-1} (for higher temperatures) and 231 kJ mol^{-1} (for lower temperatures) [13].

Illite peaks in XRD pattern are present during heating up to ~ 950 °C when begin to diminish and disappear at ~ 1050 °C [9, 14, 18]. The high-temperature reactions are accompanied with steep contraction [14, 19] and new phases are formed. A quantitative XRD analysis gave a mineralogical composition of the Füzérradvány body fired at 1080 °C: quartz (1.9 – 7.9 %), Ca-plagioclase (1.2 %), γ-alumina (9.8 – 11.9 %), mullite (4.5 – 5.8 %), K-feldspar (1.2 – 2.1 %), and amorphous phase (75.4 – 77.1 %) [14].

Elastic properties of illite determined by some authors are listed in Table 1 compiled from data given in [20 – 24]. All data in Table 1 were measured at room temperature using green illite samples. The values, with the exception of [23, 24], are calculated for illite without pores.

From the ceramic point of view, some part of illite in the kaolin-based ceramic mixture increases a content of the glassy phase as a consequence of the fluxing action of K_2O [5, 6] and decreases the firing temperature [25]. Increasing content of illite in such mixtures results in a decrease of mullite, cristobalite and quartz in the fired products [5]. Illite continues to expand up to the sintering and the shrinkage starts at the same time as vitrification. In this temperature range, the mechanical strength rapidly increases and the material becomes plastic. This is a reason why illite (or illitic clay) is preferred for a fast firing [19].

* Corresponding author. Tel.: +421-37-6408623; fax: +421-37-6408556.
E-mail address: *tomas.hulan@ukf.sk* (T. Hulan)

Table 1. Isotropic elastic modulus [GPa] and Poisson's ratio of illite

	Bulk modulus (K)	Shear modulus (G)	Young's modulus (E)	Poisson's ratio (μ)
[20]	60.1	25.3	66.6 [1]	0.316 [2]
[21]	60.2	25.4	66.8 [2]	0.315 [2]
[22]	62.2	25.7	67.8 [1]	0.319 [2]
[23]	6-12 [3]	4-6 [3]	10-15 [1]	-
[24]	-	-	10-15 [1]	-

[1] calculated from K and G as $E = 9KG/(3K + G)$,

[2] calculated from G and E as $\mu = (E/2G) - 1$,

[3] for clay generally.

As follows from the references [1 – 4, 13, 18], the main focus of the previous research was the structure of illite, its reactions to dehydroxylation and high temperature. The mechanical properties of illite during heating remain unknown. The aim of this work is experimental study of the elastic properties of illite measured in-situ during heating.

2. EXPERIMENTAL

Samples

Samples made from raw illite, supplied from the mine in Füzérradvány, were used for thermal analyses DTA, TG, TDA and mf-TMA (modulated-force thermomechanical analysis) during heating. The composition of illitic clay, as given by a supplier [25], is shown in Table 2.

Table 2. The chemical composition of illite from Füzérradvány, Hungary (in mass %)

SiO_2	Al_2O_3	Fe_2O_3	TiO_2	CaO	MgO	K_2O	Na_2O	L.O.I.
58.0	24.0	0.6	0.05	0.38	1.70	7.85	0.10	7.3

The raw illite, which was in pieces of 0.2 – 3 cm, was firstly crushed and then sieved to obtain a powder with particles not larger than 0.1 mm. Then 750 g of the powder were mixed with 250 g of the distilled water to obtain a plastic mass. Cylindrical samples were made from this mass with a laboratory extruder. After open air free drying, the samples contained ~ 3 mass % of the physically bound water and their diameter was ~ 11 mm.

A heating rate (5 °C min^{-1}) was the same for all thermal analyses. The green samples were heated in the air from room temperature up to 1100 °C, which is the presumptive highest firing temperature used in industries for building clay ceramics.

Modulated-force thermomechanical analysis (mf-TMA)

Modulated-force thermomechanical analysis, based on free vibration of the sample in a fundamental flexural mode, was used for a measurement of Young's modulus on the cylindrical samples with initial dimensions $\varnothing\, 11 \times 120$ mm during heating from 20 °C to 1100 °C with a rate of 5 °C min^{-1}. The vibrations were excited with an electromagnetic impactor and detected with a microphone. A resonant frequency of the vibrations was obtained using the fast Fourier transformation. The resonant frequency f, the length l, diameter d, and the mass m of the sample were used for calculating E according to [26, 27]. Since the ratio length/diameter = 10.9 < 20, the value of E must be multiplied with a correction coefficient T_{1c} = 1.04402 (calculated for a circular cross-section and Poisson's ratio μ = 0.3). Young's modulus at the temperature t is

$$E = 1.6774 \frac{m_0 l_0^3}{d_0^4} \frac{[1 + \Delta m(t)/m_0]}{[1 + \Delta l(t)/l_0]} f^2(t), \qquad (1)$$

where $\Delta l(t)/l_0$, $\Delta m(t)/m_0$, are relative linear thermal expansion and relative mass change of the sample measured by dilatometer and TG analyzer respectively. Deriving Eq. (1), the equal relative expansion of the sample in both directions, axial and radial, was presumed. The values l_0, d_0, m_0 are the initial length, diameter, and mass of the sample at room temperature, respectively, and $f(t)$ is the resonant frequency at the temperature t.

Differential thermal analysis (DTA), thermogravimetry (TG) and thermodilatometric analysis (TDA)

As follows from Eq. (1), the determination of E requires measuring the actual dimensions and mass of the sample during heating. This task is done by TD and TG analyses. Given the relative expansion $\Delta l(t)/l_0$, as measured by the dilatometer, and the initial dimensions l_0, d_0, the true length $l(t)$ and diameter $d(t)$ of the sample were calculated. Similarly, the true mass $m(t)$ was determined from the relative mass change $\Delta m(t)/m_0$ measured with TGA/DTA analyzer Derivatograph 1000 [28].

To reduce the temperature shift between TG, DTA, TDA and mf-TMA curves, the samples for these analyses had the same cross-section. The sample dimensions were $\varnothing\, 11 \times 40$ mm for TDA and $\varnothing\, 11 \times 20$ mm for TG and DTA. A reference compact sample for DTA had the dimensions of $\varnothing\, 11 \times 20$ mm and was made from pressed Al_2O_3 powder.

X-ray diffractometry (XRD) analysis

The XRD analysis of the powder samples was performed with the diffractometer BRUKER D8 Advance with Cu anticathode ($\lambda\alpha_1$ = 1.5406 Å), accelerating voltage 40 kV and beam current 40 mA. Data was obtained with the BRUKER LynxEye detector. The Rietveld method was used for a quantitative XRD analysis.

Evolved gas analysis (EGA)

The evolved gas analysis was performed on a powder sample (50 mg) using Setaram LabSys 1600 thermoanalyzer coupled with Pfeiffer Omnistar Mass Spectrometer in the atmosphere 79 % of Ar + 21 % of O_2 with flow rate of 60 ml min^{-1}.

Porosity

The porosity was calculated with the help of experimentally determined bulk density and matrix density. The bulk density was obtained by means of size and weight measurements of cylindrical samples. The matrix density was measured by the helium pycnometry (Pycnomatic ATC, Porotec).

3. RESULTS AND DISCUSSION

The results of the quantitative XRD analysis conducted at room temperature for the green sample and the samples fired at the temperatures 650 °C, 750 °C and 1100 °C are given in Table 3. The green sample contains illite as a main phase with an addition of 12 mass % of quartz and small amounts of montmorillonite and K-feldspar orthoclase. As the firing temperature increases, the amount of illite decreases, while the amount of muscovite and amorphous phase increases. In the sample fired at 1100 °C, no phyllosilicates are observed. The sum of parts of illite, muscovite and amorphous phase is approximately constant (80 mass % for the green sample, 80 mass % for the sample fired at 650 °C, 82 mass % for the sample fired at 750 °C and 79 mass % for the sample fired at 1100 °C). The transformation of illite at higher temperatures can be a source of muscovite [29]. The cause of the amorphous phase in the samples fired at 650 °C and 750 °C is probably also due to thermal changes of illite/muscovite. The amorphous phase in the sample fired at 1100 °C is a glassy phase. K-feldspar (orthoclase and sanidine) withstands thermal treatment and does not create the glassy phase. Mullite is also created at the highest firing temperature.

Table 3. Mineral composition of the samples in mass %

	green	650 °C	750 °C	1100 °C
Illite	80	69	34	0
Montmorillonite	4	3	4	0
Muscovite	0	7	35	0
Quartz	12	12	11	11
Orthoclase	4	5	4	2
Sanidine	0	0	0	4
Mullite	0	0	0	4
Amorphous	0	4	13	79

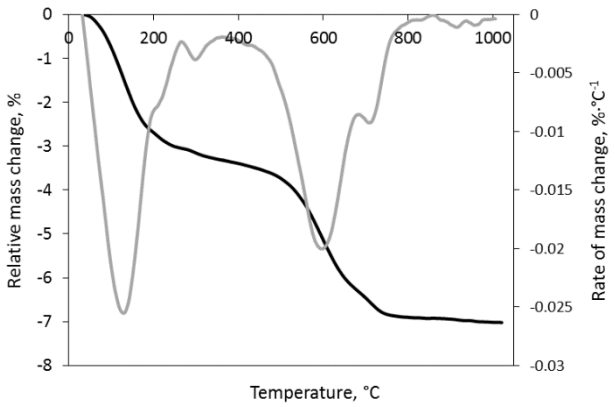

Fig. 1. Thermogravimetry of illite, TG (black line) and DTG (gray line)

The results of thermogravimetric analysis (Fig. 1.) show three steps of the decrease of the sample mass. The first step is a result of the physically bound H_2O escaping (between 20 °C and 300 °C) which occurs in two overlapping processes. The escaping of the physically bound water occurs in two overlaying processes. The first of them, which is more intensive, reaches the maximum rate at ~ 120 °C and the second one at ~ 215 °C. According to [2], a mass loss with small minimum at ~ 300 °C in the DTG curve is related to dehydration when H_2O molecules located in K-free sites of the illite interlayers are removed.

The second step is a release of the constituent water (between 400 °C and 800 °C). A dehydroxylation of illite runs in two steps which reach the maximum rate at the temperatures ~ 600 °C and ~ 700 °C being in accordance with the results showed in [13].

The results of TG are supported with the mass spectrometry (EGA) where an emission of H_2O and CO_2 were measured, see Fig. 2. EGA showed that H_2O is emitted at three clearly separate temperature intervals. The first two, which are connected with the physically bound water, are also registered in DTG and DTA curve where two overlaid processes are expressed with one intensive minimum at ~ 150 °C and one shoulder at ~ 230 °C. The dehydroxylation of illite is registered by EGA between 350 °C and 700 °C as a two-step process which is an agreement with results of TG and DTA. According to EGA, the emission of the small amount of CO_2 is also present and is caused by the burning of the organic matter in illite clay.

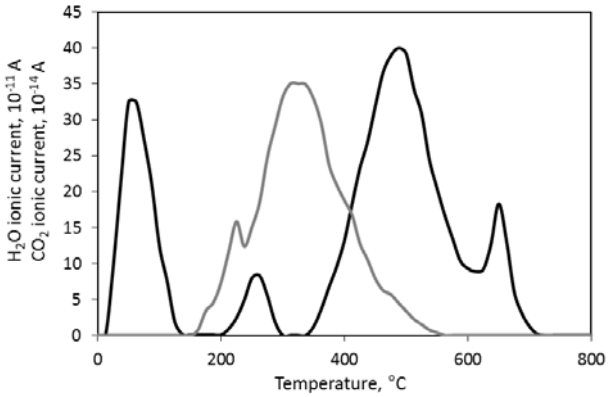

Fig. 2. Mass spectrometric results for escaping gases H_2O (black line) and CO_2 (gray line)

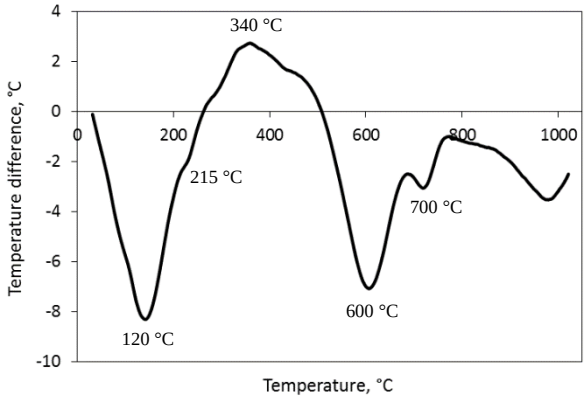

Fig. 3. DTA curve of illite

Since these processes are linked with the absorption of heat, they are represented three clear endotherms in the DTA curve with minima at 120 °C, 600 °C and 700 °C and two shoulders at ~ 215 °C and ~ 300 °C, see Fig. 3. Besides that, there is an absorption of heat above 800 °C which results in a change of metaillite into a disordered

structure and also a vitrification of the sample. An exotherm with maxima at ~ 340 °C in DTA curve is caused by the thermooxidation of organic matter.

The results of TDA in the temperature interval between 20 °C and 1100 °C are depicted in Fig. 4, where the interval between 20 °C and 400 °C is enlarged. The sample slightly expands its volume from room temperature up to ~ 500 °C (coefficient of the linear thermal expansion CLTE is $\sim 1 \times 10^{-5}\,K^{-1}$) where the dehydroxylation starts. During the dehydroxylation, the expansion becomes faster and after its completion, the expanding continues with CLTE $\sim 1 \times 10^{-5}\,K^{-1}$ up to the temperature of 900 °C. TDA also confirms two-step dehydroxylation of illite via two maxima of the CLTE, the first of them is at ~ 600 °C and the second is at ~ 700 °C. This correlates with TG and DTA. Above 900 °C, the TDA curve begins to bend downwards as a result of the sintering and vitrification [19]. Besides that, above 800 °C metaillite began to change into a disorder structure. At ~ 1100 °C, the layer structure of metaillite had been destroyed, and amorphous SiO_2 and mullite crystallite appeared [18]. These structural changes also led to the contraction of the sample. The TDA curve of the fired sample, Fig. 4, confirms a small amount of quartz via small step around 570 °C. The presence of the glassy phase exhibits itself as a contraction above 1000 °C caused by the press of the dilatometer's push-rod on the softened sample.

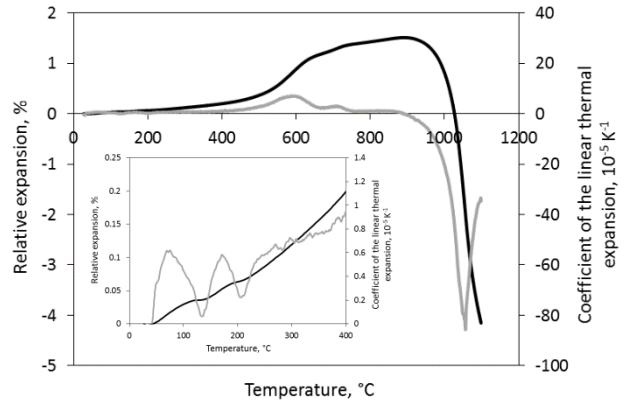

Fig. 4. Relative expansion (black line) and coefficient of the linear thermal expansion (gray line) of illite. The inset shows the interval 20 – 400 °C in greater details

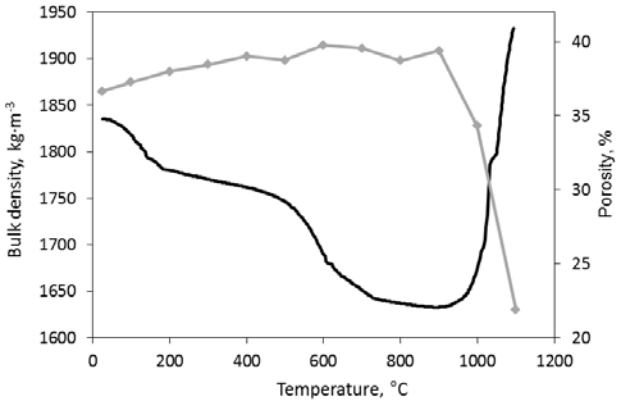

Fig. 5. Bulk density (black line) and porosity of illite (gray line)

Since *E* is proportional to a bulk density, which follows from Eq. (1), we derived this quantity from results of TG and TDA (Fig. 5.). The bulk density is determined with the mass loss up to 700 °C, which reaches ~ 7 mass % while the thermal expansion is only 1.4 %. Above 700 °C, the sample mass becomes constant and the bulk density is determined through the thermal contraction only. The contraction is caused by the sintering as noted above.

We also measured the porosity. The obtained results in Fig. 5 show that the porosity of the samples increases up to the firing temperature of 600 °C. Then a mild decrease of the porosity occurs for the samples fired at 700 °C and 800 °C followed by steep decrease of the porosity of samples fired at 1000 °C and 1100 °C, the decrease in the porosity being 17 %.

The relationship between *E*, which was calculated by Eq. (1), and the temperature *t* is depicted in Fig. 6. The first interval, which characterizes a dehydratation at low temperatures up to ~ 300 °C, is typical for samples made from clay materials. We obtained similar pictures for samples made from green electroporcelain mixtures, as well as from kaolin and illitic brick clays [30 – 32]. *E* of the samples, which had an equilibrium moisture 1 – 2 mass% after drying for a long time in the open air, is very sensitive to the loss of this water when the H_2O molecules escape from faces of the illite crystals. This process makes contacts between the crystals tighter which leads to an improvement of the elastic properties. The crystals are held together by ionic forces which are stronger when the crystals are drawn into intimate contact by the departing water films [33]. When we compare the results of mf-TMA and TDA in this low-temperature interval, we find that *E* of the sample increases while its volume also increases contrary to theoretical expectation which states that *E* is inversely proportional to the thermal expansion. We can conclude that the elastic behavior is much more influenced by properties of the boundaries between crystals than their interiors.

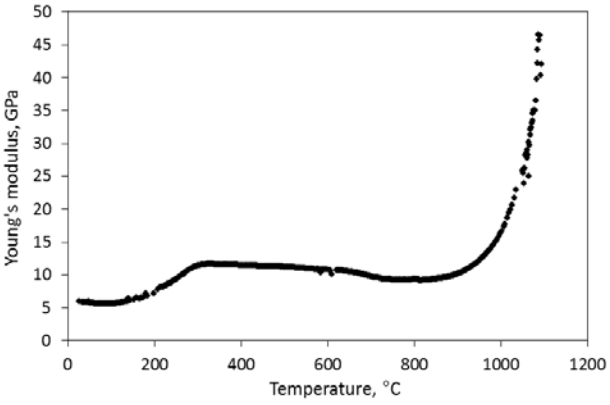

Fig. 6. Young's modulus of illite

No phase change takes place between the end of dehydration and the start of dehydroxylation. The linear decrease of *E* is caused by the weakening of the interatomic forces because the temperatures are too low for sintering. There is a good correlation with TDA results in the same temperature interval.

Above 500 °C, the dehydroxylation of illite that begins is accompanied with mass change (Fig. 1.) and thermal expansion (Fig. 4.). Dehydroxylation is reflected in *E* as a decrease of its values (Fig. 6.). It can be caused by the microporosity which results from simultaneous

increase of the volume of the sample and a decrease of its mass. It also leads to lesser values of the bulk density above 500 °C (Fig. 5.). But *E* does not decrease as dramatically as the bulk density does between 500 °C and 700 °C. In spite of the expected weakening of the metaillite crystals, *E* decreases only slightly. It also refers to a main role of the contacts between crystals which seems to be more important than mechanical properties of the crystals. And, finally, *E* exponentially increases due to sintering above 800 °C. This fact is also confirmed with TDA results.

4. CONCLUSIONS

Young's modulus of green illite from Füzérradvány (Hungary) was measured in the temperature interval 20 °C – 1100 °C and auxiliary analyses DTA, TG and TDA, XRD and EGA, were also performed. We found that:

- A removal of the physically bound water (20 °C – 250 °C) sets illite crystals closer, which leads to a significant increase of Young's modulus.
- In the next section, between the end of the escape of the physically bound water and the start of the intensive sintering (300 °C – 800 °C), the Young's modulus slightly decreases. Dehydroxylation does not significantly influence the development of Young's modulus.
- Young's modulus exponentially increases above 800 °C as a consequence of the sintering.

Acknowledgement

This work was supported by the grant VEGA 1/0646/12 from the Ministry of Education of the Slovak Republic and by the Czech Science Foundation under the project No. P105/12/G059. The authors are indebted to J. Biber from Inter-ILI Engineering Office (Hungary) for a supply of illite.

REFERENCES

1. **Stixrude, L., Peacor, D. R.** First-Principles Study of Illite-Smectite and Implications for Clay Mineral Systems *Nature* 420 2002: pp. 165 – 168.
2. **Drits, V. A., McCarty, D. K.** The Nature of Structure-Bonded H_2O in Illite and Leucophyllite from Dehydration and Dehydroxylation Experiments *Clay and Clay Minerals* 55 (1) 2007: pp. 45 – 58.
3. **Ferrari, S., Gualtieri, A. ., Grathoff, G.H., Leoni, M.** Model of Structure Disorder of Illite: Preliminary Results *Zeitschrift für Kristallographie Supplements* 23 (1) 2006: pp. 493 – 498
4. **Gualtieri, A. F., Ferrari, S., Leoni, M., Grathoff, G. H., Hugo, R., Shatnawi, M. T. M., Paglia, G., Billinge, S.J. L.** Structural Characterization of the Clay Mineral Illite-1M *Journal of Applied Crystallography* 41 2008: pp. 402 – 415. http://dx.doi.org/10.1107/S0021889808004202
5. **Ferrari, S., Gualtieri, A. F.** The Use of Illitic Clays in the Production of Stoneware Tile Ceramics *Applied Clay Science* 32 (1-2) 2006: pp. 73 – 81.
6. **Wattanasiriwech, D., Wattanasiriwech, S.** Fluxing Action of Illite and Microcline in a Triaxial Porcelain Body *Journal of the European Ceramic Society* 31 (8) 2011: pp. 1371 – 1376.
7. **Aras, A.** The Change of Phase Composition in Kaolinite- and Illite-Rich Clay-Based Ceramic Bodies *Applied Clay Science* 24 (3-4) 2004: pp. 257 – 269. http://dx.doi.org/10.1016/j.clay.2003.08.012
8. **Sedmale, G., Korovkins, A., Seglins, V., Lindina, L.** Application of Chemically Treated Illite Clay for Development of Ceramic Products *2nd International Conference on Competitive Materials and Technological Processes IOP Conf. series: Materials Science and Engineering* 47 2013: 012056.
9. **Escalera, E., Antti, M.L., Odén, M.** Thermal Treatment and Phase Formation in Kaolinite and Illite Based Clays from Tropical Regions of Bolivia *6th EEIGM International Conference on Advanced Materials Research IOP Conf. Series: Materials Science and Engineering* 31 2012: 012017.
10. **Buchwald, A., Hohmann, M., Posern, K., Brendler, E.** The Suitability of Thermally Activated Illite/Smectite Clay as Raw Material for Geopolymer Binders *Applied Clay Science* 46 (3) 2009: pp. 300 – 304.
11. **Pécskay, Z., Molnár, F., Itaya, T., Zelenka, T.** Geology and K-Ar Geochronology of Illite from the Clay Deposit at Füzérradvány, Tokaj mts., Hungary *Acta Mineralogica-Petrographica* 46 2005: pp. 1 – 7.
12. **Viczian, I.** Hungarian Investigation on the "Zempleni" Illite *Clays and Clay Minerals* 45 (1) 1997: pp. 114 – 115. http://dx.doi.org/10.1346/CCMN.1997.0450114
13. **Gualtieri, A. F., Ferrari, S.** Kinetics of Illite Dehydroxylation *Physics and Chemistry of Minerals* 33 (7) 2006: pp. 490 – 501. http://dx.doi.org/10.1007/s00269-006-0092-z
14. **Ori, R.** The Mineralogical and Technological Characterization of Illite from Füzérradvány (Hungary) as a Raw Material for Traditional Ceramics *PhD thesis, University of Modena and Emilia Region, Modena* 2003 (in Italian).
15. **Gucsik, A., Ninagawa, K., Nishido, H., Okumura, T., Bidló, A., Kovács, G., Heil, B., Patocskai, Z.** Cathodoluminiscence Microcharacterization of Illite from Füzérradvány, NE Hungary *Acta Mineralogica-Petrographica, Abstract series* 5 2006: p. 36.
16. Czechoslovak State Standard CSN 72 1083: *Thermal Analyses of Ceramic Raw Materials*.
17. **Schomburg, J., Zwar, H.** Thermal Differential Diagnosis of Mica Mineral Group *Journal of Thermal Analysis* 48 (1) 1997: pp. 135 – 139.
18. **Liu, X., Li, H., Hu, Y., Yi, D., Wang, J.** Phase Changes During Heating of Illite *TMS Annual Meeting*, San Antonio, Texas, USA 2006: pp. 309 – 316.
19. **Venturelli, C., Paganelli, M.** Sintering Behaviour of Clays for the Production of Ceramics *Ceramic Forum International Ber. DKG* 84 (5) 2007: pp. E1 – E3.
20. **Wang. Z., Wang, H., Cates, M.** Effective Elastic Properties of Solid Clays *Geophysics* 66 (2) 2001: pp. 428 – 440.
21. **Bayuk, I. O., Ammerman, M., Chesnokov, E. M.** Elastic Moduli of Anisotropic Clay *Geophysics* 72 (5) 2007: pp. D107 – D117.
22. **Katahara, K. W.** Clay Mineral Elastic Properties *66th SEG Annual International Meeting* Expanded Abstracts, Denver, Colorado, USA 1996: pp. 1691 – 1694.
23. **Vanorio, T., Prasad, M., Nur, A.** Elastic Properties of Dry Clay Mineral Aggregates, Suspensions and

Sandstones *Geophysical Journal International* 155 (1) 2003: pp. 319 – 326. http://dx.doi.org/10.1046/j.1365-246X.2003.02046.x

24. **Prasad, M., Kopycinska, M., Rabe, U., Arnold, W.** Measurement of Young's Modulus of Clay Minerals Using Atomic Force Acoustic Microscopy *Geophysical Research Letters* 29 (8) 2002: pp. 13-1 – 13-4.
25. *A Short Description of the Mining of Illite in Hungary*. Inter-ILI Mérnöki Iroda, Kosd, Hungary, 2012.
26. ASTM E1876-09: *Standard Test Method for Dynamic Young's Modulus, Shear Modulus and Poisson's Ratio by Impulse Excitation of Vibration*, ASTM International, West Conshohocken, PA, 2009.
27. ASTM C848-88: *Standard Test Method for Dynamic Young's Modulus, Shear Modulus and Poisson's Ratio for Ceramic Whiteware by Sonic Resonance*, ASTM International, West Conshohocken, PA, 2011.
28. **Podoba, R., Trník, A., Podobník, Ľ.** Upgrating of TGA/DTA Analyzer Derivatograph *Építőanyag* 64 (1-2) 2012: pp. 28 – 29.
29. **Gharrabi, M., Velde, B., Sagon, J. P.** The Transformation of Illite to Muscovite in Pelitic Rocks: Constraints from X-Ray Diffraction *Clays and Clay Minerals* 46 (1) 1998: pp. 79 – 88. http://dx.doi.org/10.1346/CCMN.1998.0460109
30. **Štubňa, I., Trník, A., Vozár, L.** Thermomechanical and Thermodilatometric Analysis of Green Alumina Porcelain *Ceramics International* 35 (3) 2009: pp. 1181 – 1185.
31. **Štubňa, I., Šín, P., Trník, A., Veinthal, R.** Mechanical Properties of Kaolin During Heating *Key Engineering Materials* 527 2013: pp. 14 – 19. http://dx.doi.org/10.4028/www.scientific.net/KEM.527.14
32. **Štubňa, I., Trník, A., Podoba, R., Sokolář, R., Bačík, P.** Elastic Propertis of Waste Calcite-Clay Ceramics During Firing *Journal of the Ceramic Society of Japan* 120 (1) 2012: pp. 351 – 354.
33. **McPhee, K. H.** An Introduction to Inorganic Dielectrics *IRE Transact, Component Parts* 6 (1) 1959: pp. 3 – 33. http://dx.doi.org/10.1109/TCP.1959.1136271